

# Effect of ultrasonically generated water vapor treatment on the Cu<sub>2</sub>ZnSnS<sub>4</sub>/CdS heterojunction-based photovoltaic cells



Myo Than Htay <sup>a,b,\*</sup>, Ryosuke Fujimura <sup>a</sup>, Remi Hasuike <sup>a</sup>, Kazushi Takei <sup>a</sup>, Noritaka Momose <sup>c</sup>, Yoshio Hashimoto <sup>a,b</sup>, Kentaro Ito <sup>a</sup>

<sup>a</sup> Department of Electrical and Electronic Engineering, Faculty of Engineering, Shinshu University, Japan

<sup>b</sup> Institute of Carbon Science and Technology, Shinshu University, 4-17-1 Wakasato, Nagano 380-8553, Japan

<sup>c</sup> Department of Electrical and Electronic Engineering, National Institute of Technology, Nagano College, 716 Tokuma, Nagano 381-8550, Japan

## ARTICLE INFO

### Article history:

Received 13 June 2015

Received in revised form

17 June 2016

Accepted 11 July 2016

Available online 9 August 2016

### Keywords:

Cu<sub>2</sub>ZnSnS<sub>4</sub>

Band alignment

Solar cell

Photovoltaic

Heterojunction

Ultrasonic spray

## ABSTRACT

The surface treatment of Cu<sub>2</sub>ZnSnS<sub>4</sub> thin films was carried out by utilizing ultrasonically generated water vapor. Suppression of the unintentional fluctuation of chemical composition near the heterointerface and enhancement in the homogeneity of CdS deposition on the Cu<sub>2</sub>ZnSnS<sub>4</sub> thin films were observed in the samples with water vapor treatment at the temperatures between 250 °C and 350 °C. The effect on the variation of conduction band and valence band offsets at the Cu<sub>2</sub>ZnSnS<sub>4</sub>/CdS heterojunction, which was observed to be in a staggered alignment, was less than ± 50 meV due to the treatment. Reproducibility of the cell characteristics was improved by the H<sub>2</sub>O spray treatment of the Cu<sub>2</sub>ZnSnS<sub>4</sub> absorbers before the deposition of CdS buffer layers. At treatment temperature of 300 °C, the improvement of efficiency by about 25% compared to that of the untreated samples was achieved.

© 2016 Elsevier B.V. All rights reserved.

## 1. Introduction

Along with various compound semiconductor materials such as GaAs, Cu(In,Ga)Se<sub>2</sub>, CdTe, and Cu<sub>2</sub>Sn<sub>1-x</sub>Ge<sub>x</sub>S<sub>3</sub>, a multinary compound of Cu<sub>2</sub>ZnSn(S,Se)<sub>4</sub> (CZTSSe) is also known as a promising absorber material for thin-film solar cell due to its properties such as earth abundance, high absorption coefficient (> 10<sup>4</sup> cm<sup>-1</sup>), and availability of various bandgaps (around 1.0–1.5 eV range) that are matching to the solar spectrum [1–15]. Up to now, the photovoltaic cell based on the heterojunction of Cu<sub>2</sub>ZnSn(S,Se)<sub>4</sub> and CdS is considered to be one of the most reliable structures and the power conversion efficiency exceeding 10% has been achieved [13–15]. On the other hand, the conversion efficiency of the cell based on the heterojunction of Cu<sub>2</sub>ZnSnS<sub>4</sub> (CZTS) and CdS is still less than 10%, which is much lower than the Shockley-Queisser limit regardless of the CZTS having a suitable bandgap of about 1.5 eV [16–21]. One of the reasons for such deficiency in the CZTS/CdS heterojunction-based cells could be due to the misalignment of energy band occurred at the interface of CZTS and CdS, which could induce the formation of defect centers causing a significant recombination of photo generated carriers [20]. Several reports on

either theoretical or experimental studies of the energy band alignment of CZTSSe-based heterojunctions also indicate the existence of energy band misalignment at the CZTS/CdS interface [22–28]. Recently, various attempts to improve the junction quality has been reported including the adjustment of Se/(Se+S) compositional ratio, utilization of alternative n-type buffer layers, and the application of surface treatment on the CZTS layer before the deposition of CdS layer [27–37]. Katagiri et al. reported about the improvement of photovoltaic performance of the CZTS/CdS solar cell by soaking the CZTS thin film into deionized water at room temperature before the deposition of CdS layer [32]. They reported that impurity phases such as oxides near the surface of CZTS thin film were removed due to the treatment so that resulting in the formation of a better CZTS/CdS heterojunction. However, fabrication of a good quality CZTS/CdS heterojunction to achieve the power conversion efficiency larger than 10% is still difficult to realize and remained as an important issue to overcome. Previously we reported a synthesis technique of a single-phase cuprite thin film utilizing ultrasonically generated water vapor, which could behave as either oxidation or reduction agent due to the presence of H<sup>+</sup> and OH<sup>-</sup> ions at high temperatures [38]. This interesting property of ultrasonically generated water vapor at high temperatures could also be useful in the selective etching of impurity phases formed unintentionally in the compound material like CZTS. In this paper, we reported the experimental results showing the effect of ultrasonically generated water vapor

\* Corresponding author at: Department of Electrical and Electronic Engineering, Faculty of Engineering, Shinshu University, 4-17-1 Wakasato, Nagano 380-8553, Japan. Fax: +81 26 269 5229.

E-mail address: [myoth@shinshu-u.ac.jp](mailto:myoth@shinshu-u.ac.jp) (M. Than Htay).

treatment on the surface of CZTS thin film under various temperatures before the deposition process of CdS buffer layer.

## 2. Experimental methods

The CZTS thin films were prepared on the Mo coated soda-lime glass (SLG, Matsunami, S-7213) substrates by a closed tube sulfurization of sputtered precursors composing of Cu, Zn, and Sn. The composition of Cu-Zn-Sn alloy target used for the preparation of precursors was set at the atomic molar percentage of Cu:Zn:Sn = 42.07:33.79:24.14, which can also be expressed in the Cu/(Zn+Sn) ratio as 0.73 and Zn/Sn ratio as 1.4. In order to investigate the photovoltaic characteristics of the cells, the precursors prepared from the Cu-Zn-Sn alloy target with the atomic molar composition of Cu:Zn:Sn = 45:30:25, which is equivalent to Cu/(Zn+Sn) = 0.82 and Zn/Sn = 1.2, were also used. The sulfurization process was carried out under the sulfur pressure of 1.5 atm at 590 °C. The details of temperature profile of the sulfurization process is shown in Fig. 1. The surface treatment of CZTS was carried out in our original ultrasonic spray pyrolysis system at the temperatures between 250 and 350 °C for 15 min, the structural details of which was described in our previous reports [37–40]. Vapor of the deionized water (18.2 MΩ cm at 25 °C), which was generated by the ultrasonic vibration of 2.4 MHz, was used for the surface treatment of CZTS. The generated water vapor was transported to the CZTS absorber thin films placed inside a reaction chamber by means of N<sub>2</sub> carrier gas, the flow rate of which was adjusted at 1.0 L/min. The temperature of the sample was adjusted by an infrared-gold-image furnace (ULVAC, E-25), where the samples to be reacted were placed inside a graphite susceptor for indirect heating. Before and after the surface treatment process, a pre-evacuation and post-evacuation of the reaction chamber were carried out in order to purge unintended oxygen contamination of the ambient during the heating and cooling processes.

An X-ray diffractometer (XRD, Rigaku, RINT-2200 V/PCSV, CuK $\alpha$  ray,  $\lambda = 1.5418 \text{ \AA}$  with a Bragg-Brentano  $\theta - 2\theta$  geometry at 40 kV, 30 mA) was used for confirming the crystalline properties of the absorber thin films. For the Raman spectroscopy analyses, a laser Raman spectrometer (COMET-3504) equipped with an Nd:YVO<sub>4</sub> SHG Laser (continuous wave of  $\lambda = 532.3 \pm 0.3 \text{ nm}$  and maximum power of 500 mW) and a monochromator (SOL instrument, MS-3504I) was used. The spectral resolutions of the system is  $\pm 0.045 \text{ nm}$  for the grating of 2400 lines/mm. The measurement spectra were obtained in the backscattering geometry and were captured by a CCD detector (ANDOR iDUS, DU420A-BR-DD, pixel size of 14  $\mu\text{m}$ ). For evaluating the surface morphology of the absorber thin films, a field emission scanning electron microscope

(FE-SEM, Hitachi, S-4100) was used. A four-probe method (Kyowa Riken, K89PS, tips gap: 1 mm) was applied for measuring the resistivity of the samples in rectangular shape of  $15 \times 10 \text{ mm}^2$  in size, which were deposited directly on the SLG substrates. An electron probe microanalyzer (EPMA, Shimadzu, EPMA-1610) was used to measure the final bulk composition of the films and their corresponding elemental mapping. An X-ray photoelectron spectrometer (XPS, Surface Science Instruments, S-probe 7339, Al K $\alpha$  1486.6 eV source with a hemispherical energy analyzer) was used to evaluate the composition of the surface of the samples as well as the energy band alignment of the CZTS/CdS heterojunctions. In order to measure the difference of core energy levels directly, the shallow CZTS/CdS junctions were fabricated by the chemical bath deposition of 3 nm-thick CdS layer on the CZTS thin film, from which the photoelectron signals from both layers of CZTS and CdS can be observed simultaneously. The details of energy band alignment measurement method were reported elsewhere [41]. Calibration of the binding energy scale of the XPS system was performed by referencing the values of Au 4f<sub>7/2</sub> and Cu 2p<sub>3/2</sub> spectra measured under the same condition. A spectrophotometer (Shimadzu, UV-3100) was used to measure the transmittance and the optical bandgap of the CZTS and CdS thin films deposited directly on the SLG substrates. The photovoltaic characteristic measurements were carried out under irradiance of 1000 W/m<sup>2</sup> at AM 1.5 spectrum (Wacom, HX-504). Measurements of the external quantum efficiency were carried out by the spectrophotometer (Shimadzu, UV-3100) interfaced with a lock-in amplifier (EG & G Princeton applied research, Model-5210) utilizing a reference signal obtained from a standard Si photodiode (Hamamatsu, S-1337). The photovoltaic cell as shown in the inset of Fig. 1 was completed by chemical bath deposition of a CdS layer (about 60 nm in thickness) on the CZTS absorber thin film (about 2.0  $\mu\text{m}$  in thickness) with or without water vapor treatment process, followed by the RF magnetron sputtering of a non-doped In<sub>2</sub>O<sub>3</sub> target (purity 99.99%) under pure Ar ambient without heating the substrate to achieve a top transparent electrode thin film (about 400 nm in thickness), the resistivity of which was about  $3 \times 10^{-4} \Omega \text{ cm}$ , on top of the CdS layer.

## 3. Results and discussion

The XRD patterns of the samples before and after the water vapor treatment at various conditions are compared in Fig. 2. All the samples exhibit diffraction patterns which are in good agreement with the JCPDS pattern of 26–0575. The strongest peak due to the diffraction from (112) planes of the Kesterite phase is also observed in all the samples. The diffraction peaks due to impurity phases are not apparently detected except that of the Mo from the back electrode. However, the vibration modes due to ZnS phase is weakly observed in the Raman spectra as shown in Fig. 3, which is in good agreement with the other report [42]. There is no obvious change in the XRD diffraction peaks after the treatment process at the temperatures of 250 °C, 300 °C, and 350 °C. Difference in the Raman spectra due to the water vapor treatment is also not distinguish as shown in Fig. 3. This implies that the water vapor treatment does not give rise to major transformation in the crystalline structure of the bulk of CZTS thin films. In Fig. 4, the SEM images of the surface of CZTS thin films before and after the water vapor treatment are shown in comparison. There are no distinct changes in the surface morphology of CZTS thin films after the treatments at the temperatures of 250 °C, 300 °C, and 350 °C. This result is consistent with the XRD and Raman data shown in Figs. 2 and 3. The average values of electrical resistivity of the CZTS thin films before and after the water vapor treatment are shown in

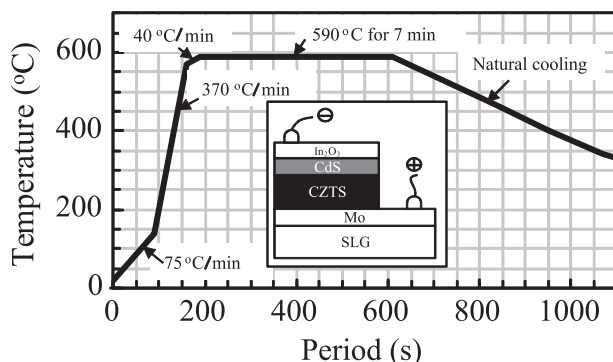


**Fig. 1.** The temperature profile of a closed tube sulfurization process of the precursors under sulfur pressure of 1.5 atm. The inset shows a schematic of the CZTS/CdS heterojunction-based cell structure. The thicknesses of the films are not drawn to scale.

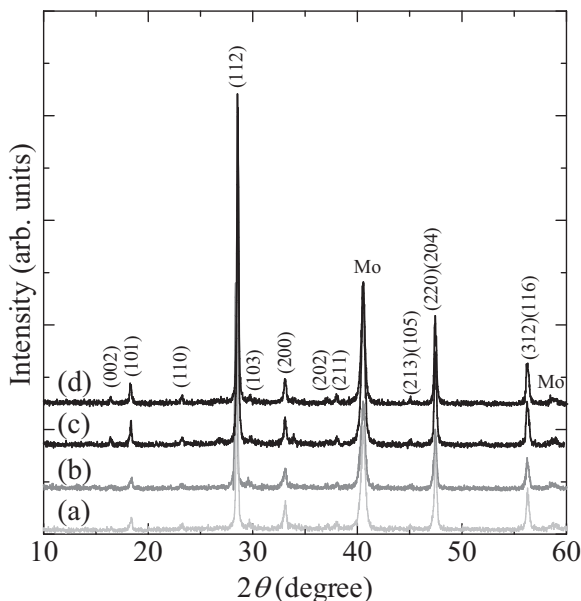


**Fig. 2.** The XRD patterns of CZTS thin films deposited on the Mo coated SLG substrates (a) without  $\text{H}_2\text{O}$  vapor treatment, (b) with  $\text{H}_2\text{O}$  vapor treatment at  $250^\circ\text{C}$ , (c)  $300^\circ\text{C}$ , and (d)  $350^\circ\text{C}$ , respectively. Baseline offset is adjusted to enhance the visual of the patterns.

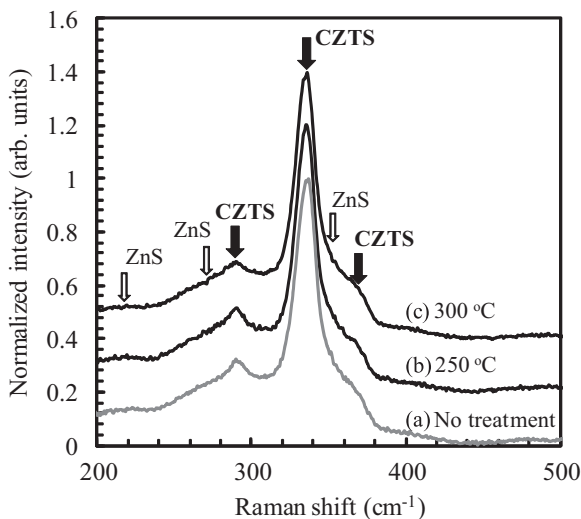


**Fig. 3.** The Raman spectra of the samples (a) without water vapor treatment, (b) with water vapor treatment at  $250^\circ\text{C}$ , and (c)  $300^\circ\text{C}$ , respectively. Black arrows indicate the main vibration modes of CZTS phase and open-arrows show that of impurity ZnS phase. All the spectra are normalized with their most prominent peak observed in the  $200\text{--}500\text{ cm}^{-1}$  range. The corresponding baseline offset is also made for visual enhancement.

**Table 1.** The treatment does not cause any obvious change in the resistivity, which is kept almost constant at  $1.6 - 1.7 \times 10^3 \Omega \text{ cm}$ . The comparison of optical bandgap deduced from the extrapolation of  $(ah\nu)^2$  vs.  $h\nu$  plot is shown in Fig. 5. It is found that the bandgap is about 1.5 eV for all the samples and the difference due to the water vapor treatment is indistinguishable. Here, the absorption coefficient  $\alpha$  was estimated from the transmittance and reflectance spectra of the corresponding CZTS thin film (about 1  $\mu\text{m}$  thick) deposited directly on the SLG substrate. The reflections of all the samples were less than 2% and no obvious difference due to the treatment was detected.

Before analyzing the effect of water vapor treatment on the bulk chemical composition, it is important to investigate the amount of deviation from stoichiometry in the sulfurized CZTS

thin films before the water vapor treatment. It is found that the ratios of  $\text{Cu}/(\text{Zn}+\text{Sn})$ ,  $\text{Zn}/\text{Sn}$ , and  $(\text{Cu}+\text{Zn}+\text{Sn})/\text{S}$  of the sulfurized CZTS thin films before the water vapor treatment used in this experiment were varied between 0.79–0.88, 1.28–1.34, and 0.98–1.04, respectively. By comparing the resultant compositional ratios of sulfurized CZTS thin films without water vapor treatment to their corresponding precursors (i.e., 0.73 for  $\text{Cu}/(\text{Zn}+\text{Sn})$  and 1.4 for  $\text{Zn}/\text{Sn}$  ratios before sulfurization), it is revealed that the ratio of  $\text{Cu}/(\text{Zn}+\text{Sn})$  is increased by about 5–18% while that of the  $\text{Zn}/\text{Sn}$  is decreased by about 10% after the sulfurization process. This result indicates that re-evaporation of either Zn or Sn species takes place during the sulfurization process. It is also noted that the amount of re-evaporation of Zn is much higher than that of Sn since the  $\text{Zn}/\text{Sn}$  ratio of sulfurized CZTS thin films is reduced to nearly 1.3, which was set at 1.4 in their precursors. The bulk chemical compositional ratios of these CZTS thin films before and after the water vapor treatment measured by EPMA are shown in Fig. 6. Since all the plots in the Fig. 6 are found within the region bounded by the dash-lines that satisfied  $y = x \pm 0.05$  correlation, it indicates that the changes in the bulk compositional ratios due to the water vapor treatments are less than  $\pm 5\%$ , which corresponds to the resolution limit of EPMA measurement. The amount of changes for  $\text{Cu}/(\text{Zn}+\text{Sn})$  and  $\text{Zn}/\text{Sn}$  ratios due to the sulfurization process before water vapor treatment are significantly larger than that of the water vapor treatment process. Hence, re-evaporation during the sulfurization process could be a main reason for obvious compositional fluctuation in the final CZTS thin films, which will vary the photovoltaic characteristics as a consequence. The  $(\text{Cu}+\text{Zn}+\text{Sn})/\text{S}$  ratios are observed to be near  $1.0 \pm 0.05$ , which indicates that the cation-to-anion ratio of water vapor-treated CZTS thin films are close to the stoichiometric value of unity.

For further detailed analysis, the bulk elemental mapping of CZTS thin films before and after the water vapor treatment at various conditions as well as that of their corresponding CZTS/CdS heterojunctions was carried out by EPMA as shown in Fig. 7(a)–(x). The mapping results of each element such as Cu, Zn, Sn, S, Cd, and O of the sample without water vapor treatment are shown in Fig. 7(a)–(f), respectively. By comparing the distribution of Cu, Zn, and Sn of the CZTS thin film with no treatment before the deposition of CdS buffer layer as shown in Fig. 7(a)–(c), it is observed that the Cu and Sn are located in the same distribution profile, while Zn is distributed in a reverse correlation to that of Cu and Sn. From this result, it could be considered that there is a localized Zn dominant phase such as ZnS either in the bulk or on the surface of the CZTS thin film with Zn-excess composition, which is also observed in the Raman spectra as shown in Fig. 3. The mapping results for the samples with water vapor treatment at different temperatures such as  $250^\circ\text{C}$ ,  $300^\circ\text{C}$ , and  $350^\circ\text{C}$  before the deposition of CdS buffer layer are also shown in Fig. 7(g)–(j), (m)–(p), and (s)–(v), respectively. It is clearly observed that homogeneity of the distribution of compositional elements in these samples are relatively high compare to the one with no treatment. By comparing the distribution of Cd in each sample after the formation of CZTS/CdS heterojunctions as shown in Fig. 7(e), (k), (q), and (w), relatively homogeneous distribution of Cd is found in all the samples with water vapor treatments. This results indicate that the water vapor treatment has obvious effect on reducing irregular deposition of CdS layers on the CZTS thin films. The difference in the distribution of oxygen, which could be present due to the oxidation reaction of CZTS with water vapor during the treatment, is not clearly identified since the signal intensities are too weak as shown in Fig. 7(f), (l), (r), and (x), respectively. The result of a detailed mapping correlation of Cd in CdS layer with respect to the compositional elements of CZTS such as Cu, Zn, and Sn lying beneath the heterojunction without water vapor treatment is described in Fig. 8. It is observed that there are two distinct regions where different compositional distributions are

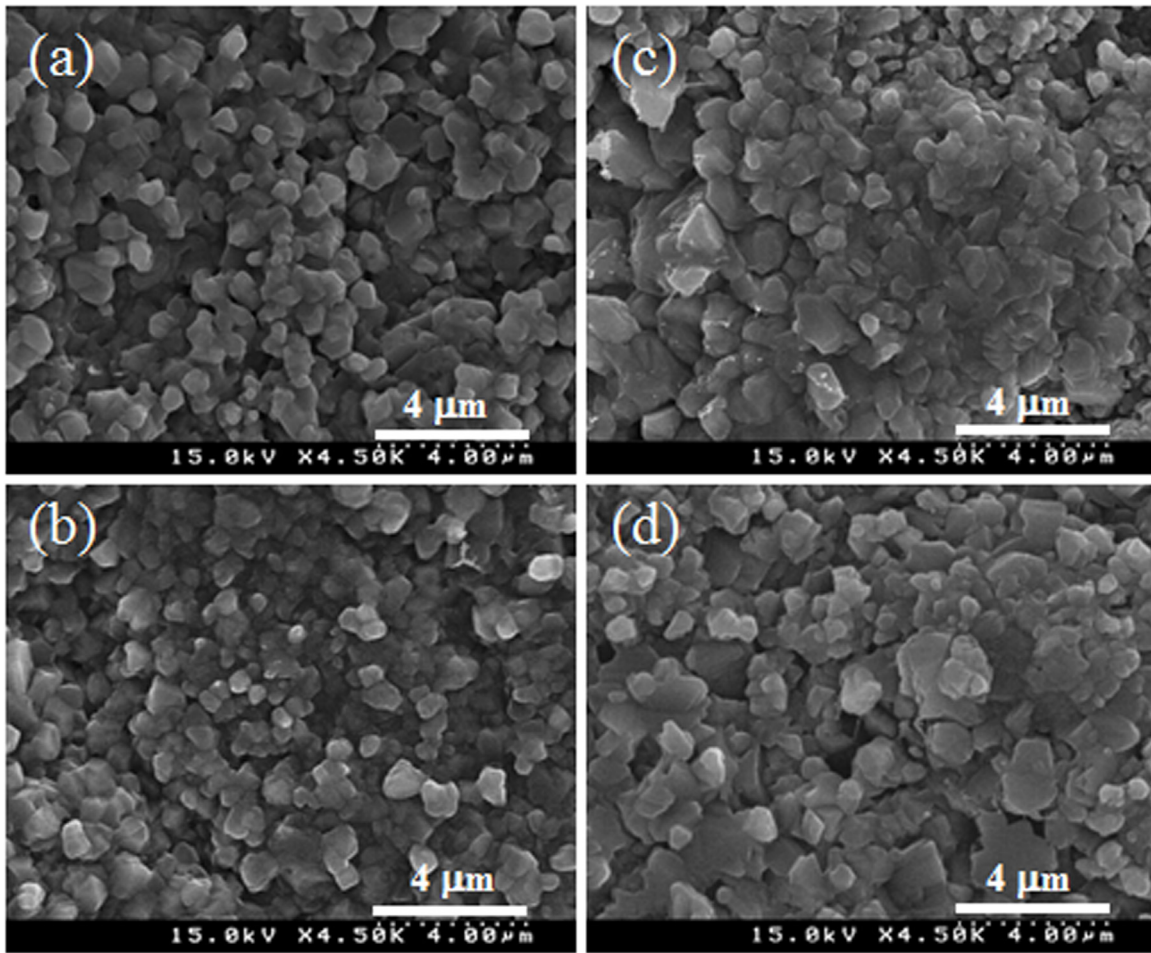


**Fig. 4.** The SEM images of CZTS thin films deposited on the Mo coated SLG substrates (a) without  $\text{H}_2\text{O}$  vapor treatment, (b) with  $\text{H}_2\text{O}$  vapor treatment at  $250\text{ }^\circ\text{C}$ , (c)  $300\text{ }^\circ\text{C}$ , and (d)  $350\text{ }^\circ\text{C}$ , respectively.

**Table 1**

The resistivity of CZTS thin films and the energy band discontinuity of CZTS/CdS heterojunctions obtained after various conditions of water vapor treatment.

Sample conditions	Resistivity ( $\Omega \text{ cm}$ )	VBM offset $\Delta E_v$ (eV)	CBM offset $\Delta E_c$ (eV)
No treatment	$1.67 \times 10^3$	$1.24 \pm 0.05$	$-0.33 \pm 0.05$
$250\text{ }^\circ\text{C}$	$1.56 \times 10^3$	$1.22 \pm 0.05$	$-0.31 \pm 0.05$
$300\text{ }^\circ\text{C}$	$1.70 \times 10^3$	$1.20 \pm 0.05$	$-0.29 \pm 0.05$
$350\text{ }^\circ\text{C}$	$1.60 \times 10^3$	Not measured	Not measured

detected as highlighted by the dash-lines in Fig. 8(a) and (b). In the first region denoted as 1, the concentration of Cd is relatively higher than in the surrounding area. In the case of second region described as 2, relatively high density of Zn is observed, which could be considered as the region dominant by the presence of ZnS phase. It is also found that the distributions of Cd and Zn are in reverse correlation to each other. This result indicates that the growth rate of CdS thin film is higher at the surface where the CZTS phase is located, while relatively slower deposition of CdS layer is taken place at the regions with Zn-excess phase such as ZnS during the chemical bath deposition process. In other words, it could be said that the heterogeneous nature of the surface of CZTS thin films with no water vapor treatment could induce irregular reactions, which could result in the formation of uneven CdS layer during the chemical bath deposition process.

In order to clarify the chemical composition of surface to that of the bulk, the result of XPS analysis is shown in Fig. 9. As shown in

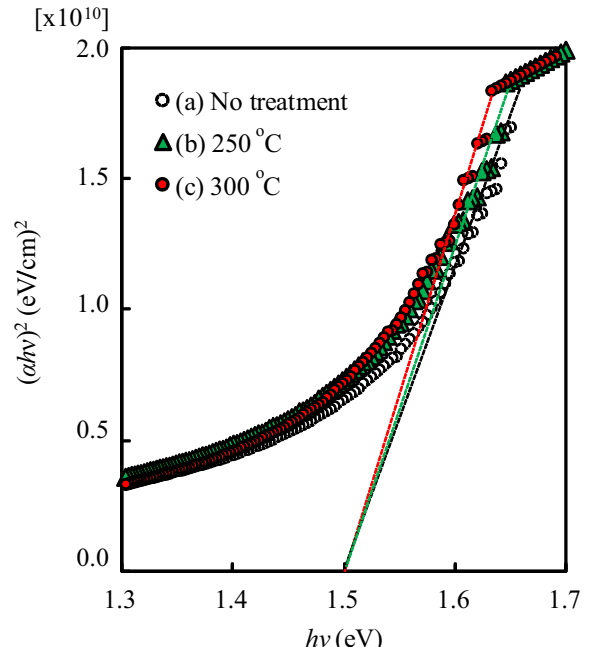


**Fig. 5.** The estimation of optical bandgap of the samples (a) without  $\text{H}_2\text{O}$  vapor treatment, (b) with  $\text{H}_2\text{O}$  vapor treatment at  $250\text{ }^\circ\text{C}$ , and (c)  $300\text{ }^\circ\text{C}$ , repectively. The dash-lines indicate the extrapolation of the corresponding straight line portion of the  $(ahv)^2$  vs.  $h\nu$  plots.

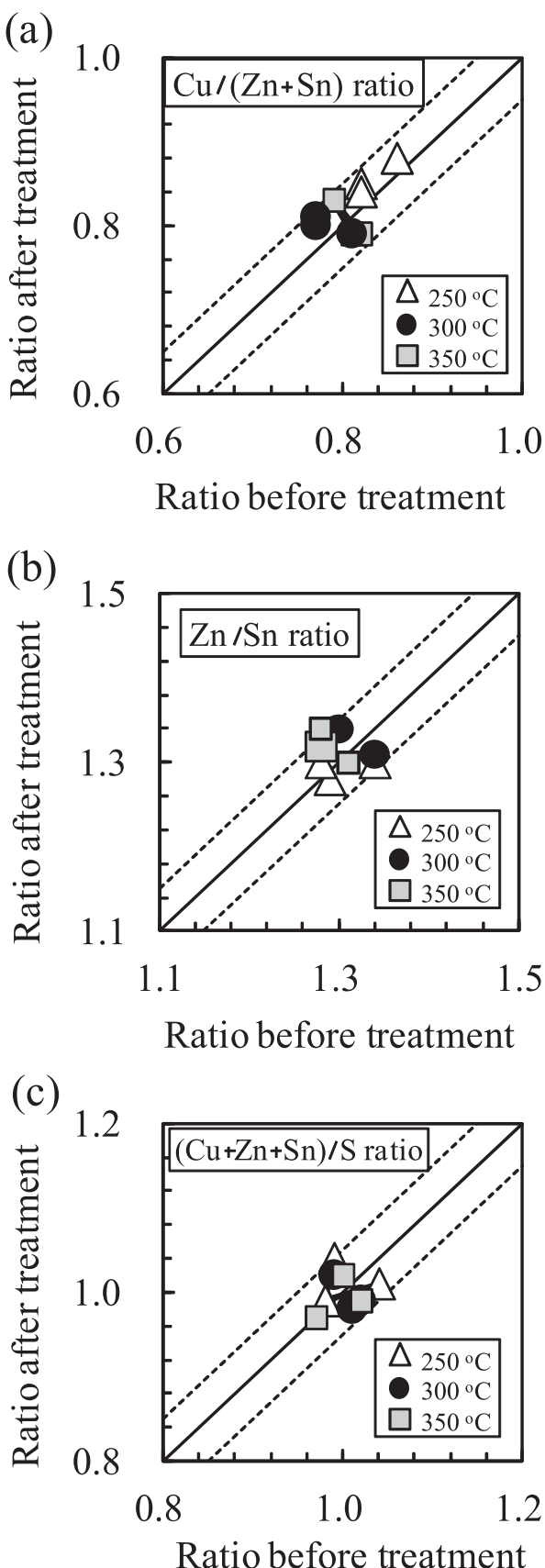


**Fig. 6.** The bulk chemical compositional ratios of (a)  $\text{Cu}/(\text{Zn}+\text{Sn})$ , (b)  $\text{Zn}/\text{Sn}$ , and (c)  $(\text{Cu}+\text{Zn}+\text{Sn})/\text{S}$  of the CZTS thin films before and after water vapor treatment at various temperatures such as 250 °C, 300 °C, and 350 °C. The horizontal (vertical) axis shows the corresponding chemical compositional ratio of the CZTS thin films before (after) the treatment in each graph. The region between the dash-lines in each graph describes the variation of compositional ratio less than 5%.

**Fig. 9(a)**, it is found that the ratio of  $\text{Cu}/(\text{Zn}+\text{Sn})$  is varied between 0.2–0.3, which is much smaller than the bulk value of 0.79–0.88. This result indicates that the surface of CZTS thin film within a depth of a few nanometers is depleted in Cu. In other words, there could be Zn or Sn rich phases containing  $\text{ZnS}$  or  $\text{SnS}_2$  at the surface of CZTS thin films. Since the final bulk composition of all the samples were confirmed to be in the Zn-excess condition by EPMA, i.e., the ratio of  $\text{Cu}/(\text{Zn}+\text{Sn})$  is smaller than 1.0 while that of the  $\text{Zn}/\text{Sn}$  is greater than unity, it is reasonable to consider that the existence of Zn-excess phase such as  $\text{ZnS}$  near the surface is more likely. It is also confirmed that the  $\text{Cu}/(\text{Zn}+\text{Sn})$  ratios of the samples with water vapor treatment are smaller than that of the sample without the treatment. It is found that the higher the treatment temperature, the smaller is the  $\text{Cu}/(\text{Zn}+\text{Sn})$  ratio. This could be due to efficient removing of Cu-rich species near the surface by the water vapor treatment at high temperatures. In the case of  $\text{Zn}/\text{Sn}$  ratio as shown in **Fig. 9(b)**, it is observed that this ratio is increased to the values larger than 1.5, which was between 1.28 and 1.34 for the bulk of the CZTS thin films. This result also implies that the composition of Zn is the most dominant at the surface of CZTS thin film. In addition, a large fluctuation of the  $\text{Zn}/\text{Sn}$  ratio (varying between 1.52 and 2.48) is observed in the samples without water vapor treatment, while that of the samples with water vapor treatment exhibit relatively homogeneous compositional ratio. For the samples with treatment at 250 °C, the  $\text{Zn}/\text{Sn}$  ratio is stable near 2.12, while that of the samples with treatment at 300 °C is observed to be converged near 1.58. From this result, it could be considered that the water vapor treatment has the effect of converging the  $\text{Zn}/\text{Sn}$  ratio of the CZTS surface to a specific value depending on the treatment temperature. The compositional ratio of  $(\text{Cu}+\text{Zn}+\text{Sn})/\text{S}$  is observed to be varying between 0.8 and 1.1 and obvious difference between the samples with and without water vapor treatment is not found as shown in **Fig. 9(c)**. The molar ratio of oxygen observed at the surface is measured to be varied between 6.7–12.1% for the samples without treatment, 14.9–16.5% for the samples with treatment at 250 °C, and 18.7–19.0% for the treatment at 300 °C, respectively. This result indicates that the surface oxidation takes place in all the samples and is accelerated in the samples by the water vapor treatment at higher temperatures. In the case of the sample without the treatment, however, unintended oxidation takes place unevenly so that the fluctuation of oxygen concentration at the surface is larger than that of the other samples with water vapor treatment. The  $\text{Cu } 2p_{3/2}$ ,  $\text{O } 1s$ ,  $\text{Zn } 3p_{3/2}$ , and  $\text{Sn } 3d_{5/2}$  peaks of the samples with and without the treatment are shown in **Fig. 10(a)–(d)**, respectively. In the samples with water vapor treatment, an obvious chemical shifting of the  $\text{Cu } 2p_{3/2}$  peak toward higher binding energy side is observed, while the peak of  $\text{O } 1s$  is shifted toward lower energy side comparing to the peaks of the sample without treatment. On the other hand, the shifting of  $\text{Zn } 3p_{3/2}$ , and  $\text{Sn } 3d_{5/2}$  peaks are too small to be distinguished clearly. This chemical shifting could be interpreted as the existence of oxidation reaction near the surface. By taking account of the experimental results of both the compositional mapping of EPMA and the surface analysis of XPS, the water vapor treatment is considered to be effective for reducing the compositional fluctuation near the surface of the CZTS thin film, where the formation of homogeneous CdS deposition could be realized with high reproducibility.

In order to investigate the effect of water vapor treatment on the energy band alignment at the CZTS/CdS heterojunction, measurement by XPS was carried out for the samples without treatment as well as the samples with treatment at 250 °C and 300 °C, respectively. In **Fig. 10(e)**, the XPS spectra taken near the valence band maximum (VBM) of the CZTS of various treatment conditions

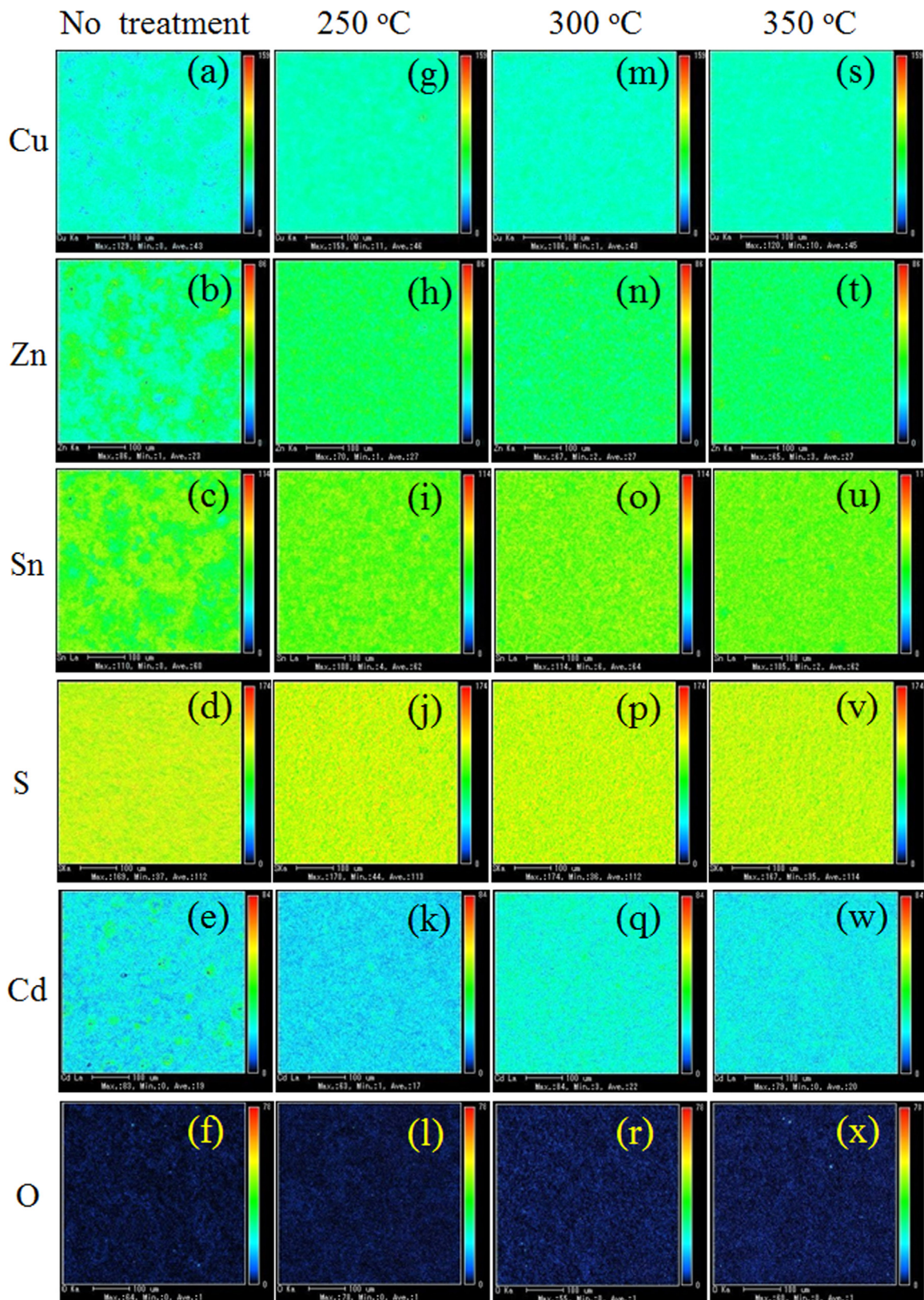


**Fig. 7.** The results of elemental mapping of the CZTS thin films with various conditions and the corresponding CZTS/CdS heterojunctions by EPMA. (a)–(f) show the mapping of spatial distribution of the Cu, Zn, Sn, S, Cd, and O of the sample without water vapor treatment, (g)–(l) describe that of the sample with treatment at 250 °C, (m)–(r) represent that of the sample with treatment at 300 °C, and (s)–(x) depict that of the sample with treatment at 350 °C, respectively. The area of elemental mapping is 500 × 500  $\mu\text{m}^2$ .

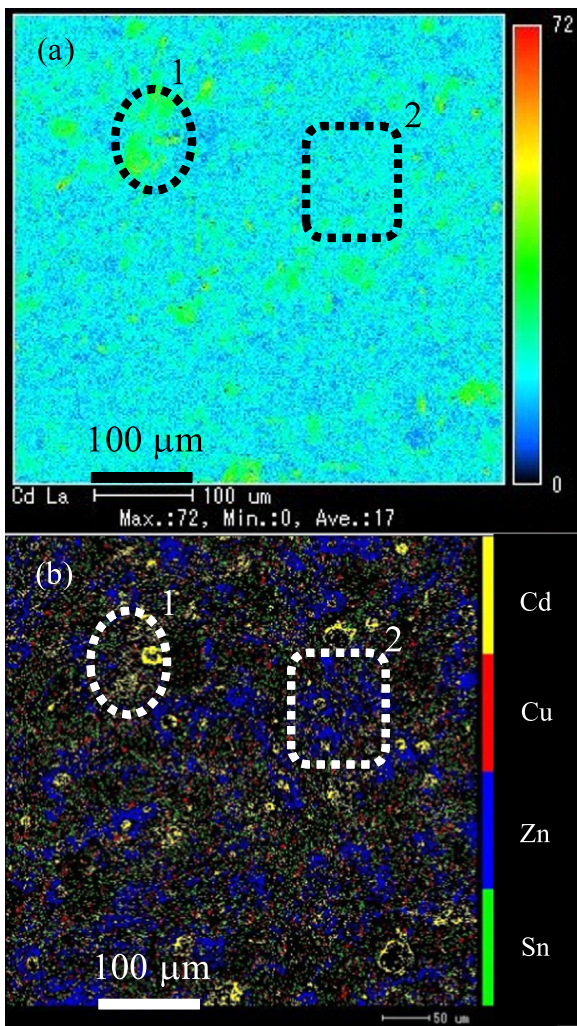


**Fig. 8.** The mapping correlation of the Cd in the CdS buffer layer to the distribution of Cu, Zn, and Sn in the CZTS thin film of the CZTS/CdS heterojunction without water vapor treatment. (a) shows the distribution of deposited Cd and (b) describes the location of each element such as Cu, Zn, and Sn of the CZTS thin film along with that of the Cd of the CdS buffer layer. The regions denoted as 1 in the images highlight the locations where high density of Cd distribution is observed and the regions within the rectangular boxes denoted as 2 show the locations where Zn is observed in high density.

are shown in comparison with that of the CdS. It is found that the VBMs of the samples with water vapor treatment are observed at slightly deeper energy sides than that of the sample with no treatment. The higher the treatment temperature, the larger is the shifting of VBM. For determining the core levels difference, Zn 3d and Cd 4d peaks of the shallow CZTS/CdS junctions were used. The results of valence band and conduction band discontinuity are described in Table 1, which were deduced from the following Eqs. (1) and (2).

$$\Delta E_V = \Delta E_{CL} + E_{V-Zn3d} - E_{V-Cd4d} \quad (1)$$

$$\Delta E_c = E_g(CdS) - E_g(CZTS) - \Delta E_V \quad (2)$$

Here,  $\Delta E_V$  and  $\Delta E_c$  are the valence band and conduction band discontinuity or offset,  $\Delta E_{CL}$  is denoted for the core levels difference of Zn 3d and Cd 4d peaks of the CZTS/CdS heterojunction,  $E_{V-Zn3d}$  and  $E_{V-Cd4d}$  represent the energy levels of Zn 3d and Cd 4d measured from the corresponding VBM of CZTS and CdS,  $E_g(CdS)$  and  $E_g(CZTS)$  are the bandgap of CdS and CZTS, respectively. For

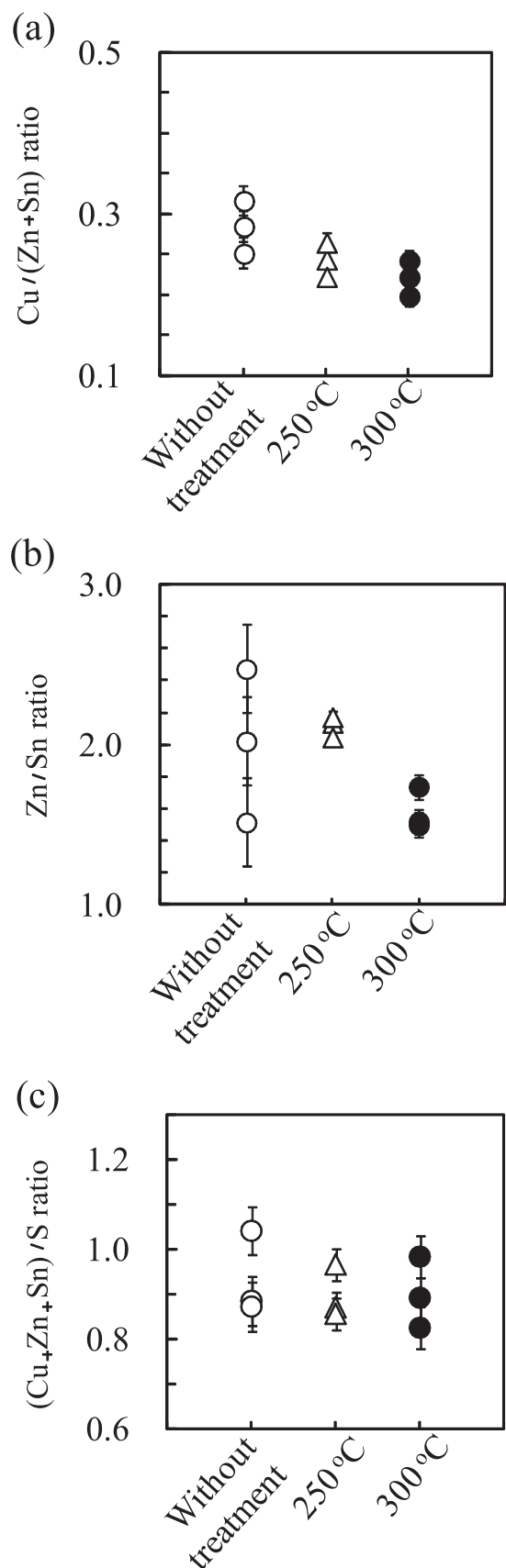


**Fig. 9.** The surface chemical compositional ratios of (a) Cu/(Zn+Sn), (b) Zn/Sn, and (c) (Cu+Zn+Sn)/S of the CZTS thin films before and after water vapor treatment at the temperatures of 250 °C and 300 °C.

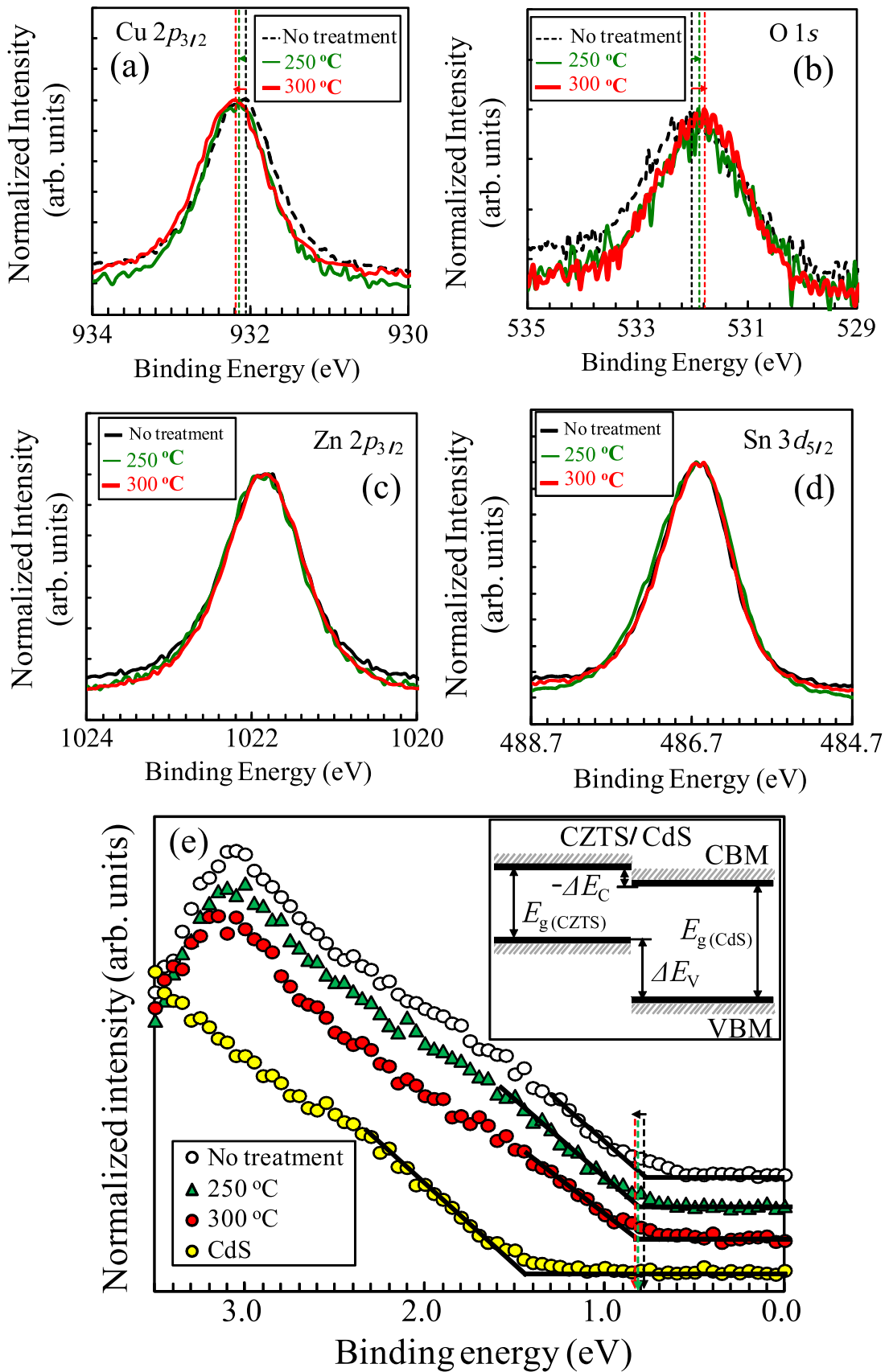


**Fig. 10.** The XPS spectra of (a) Cu 2p<sub>3/2</sub>, (b) O 1s, (c) Zn 3p<sub>3/2</sub>, (d) Sn 3d<sub>5/2</sub> peaks of the CZTS thin films with and without water vapor treatment, and (e) the spectra near the valance band edge of CdS and CZTS with and without the treatment. The inset of (e) describes the possible energy band alignment of CZTS/CdS heterojunction. The spectra in all the figures (a)–(e) are normalized with respect to their corresponding prominent peak and the baseline offset in (e) is made for visual enhancement. Note that the schematic energy levels of the energy band alignment shown in the inset of (e) are not drawn to scale.

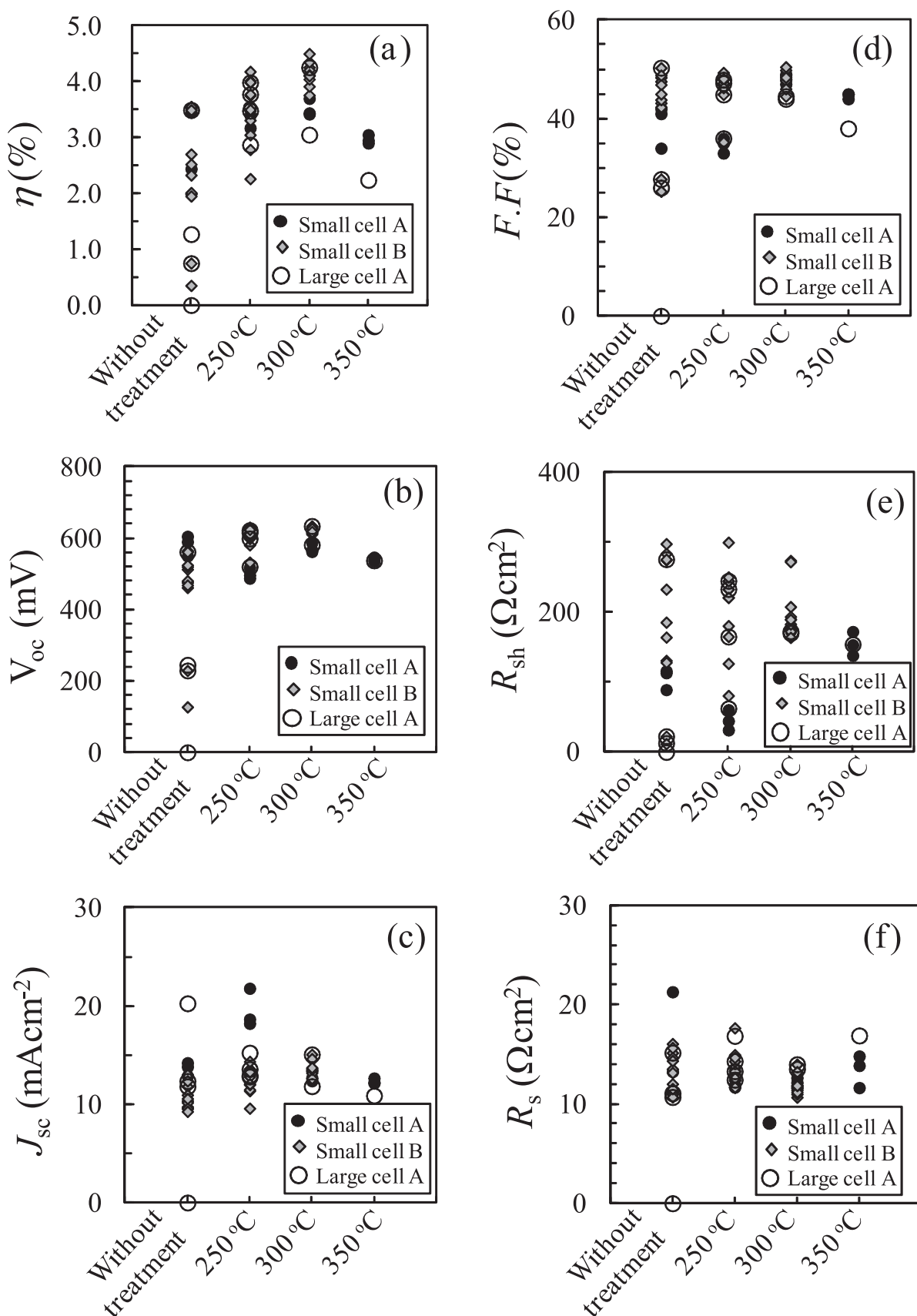


**Fig. 11.** The photovoltaic characteristics of the samples with and without water vapor treatment: (a) conversion efficiency,  $\eta$ , (b) open-circuit voltage,  $V_{oc}$ , (c) short-circuit current density,  $J_{sc}$ , (d) fill factor,  $FF$ , (e) shunt resistance,  $R_{sh}$ , and (f) series resistance,  $R_s$ . The data for the cells A (using target having chemical ratios of  $Cu/(Zn+Sn) = 0.73$  and  $Zn/Sn = 1.4$ ) with larger (smaller) active area are plotted in larger open-circle (filled-circle). The data for the cells B prepared from the target with chemical ratios of  $Cu/(Zn+Sn) = 0.82$  and  $Zn/Sn = 1.2$  are plotted in diamond.

$\Delta E_c$ , positive (negative) value is used to express the energy band offset when conduction band minimum (CBM) of CZTS is lower (higher) than that of CdS. A reciprocal assignment is applied for  $\Delta E_v$ , i.e., positive when VBM of CZTS is higher than that of CdS and vice versa. From the results shown in Table 1, it is found that  $\Delta E_v$  is positive and  $\Delta E_c$  is negative for all the samples. This implies that all the CZTS/CdS heterojunctions are aligned in a staggered structure, which is also known as type-II heterojunction, as shown in the inset of Fig. 10(e). This observation is in good agreement with the data of the other reports qualitatively though there are some differences in the amount of offset [22–28]. In comparing the energy band alignment of the samples with water vapor treatment to the one with no treatment, tendency of decreasing in the discontinuity of both  $\Delta E_c$  and  $\Delta E_v$  is observed in the formers although the amount of change is less than 0.05 eV, which is insignificant over the resolution limit of the XPS measurement system. In other words, it could be said objectively that the variation of band offsetting at the VBM and CBM is relatively small and the amount of increasing or decreasing of discontinuities larger than 50 meV is not likely by the water vapor treatment. Accordingly, it is reasonable to think from these results that the oxidation caused by water vapor treatment near the surface of CZTS could lead to suppressing the fluctuation of chemical composition, while the effect on the variation of discontinuity of VBM and CBM at the CZTS/CdS heterojunction is smaller than 50 meV.

In Fig. 11, the photovoltaic characteristics of the cells with various conditions of water vapor treatment are shown in comparison to the one with no treatment. The comparison between the characteristics of the cells with small active area ( $4 \text{ mm}^2$ ) and large active area ( $25 \text{ mm}^2$ ) are also made in order to analyze the effect of the spatial compositional distribution on the photovoltaic characteristics. In addition, the characteristics of two types of cells utilizing absorber layers prepared from alloy targets with different chemical compositions are also compared in order to investigate the changes caused by variation of the bulk chemical composition. The samples prepared from the alloy target having chemical ratios of  $\text{Cu}/(\text{Zn}+\text{Sn}) = 0.73$  and  $\text{Zn}/\text{Sn} = 1.4$  are denoted as A in Fig. 11. On the other hand, those from the target with  $\text{Cu}/(\text{Zn}+\text{Sn}) = 0.82$  and  $\text{Zn}/\text{Sn} = 1.2$  are described as B, in which the content of Zn is lower and closer to the stoichiometric composition than that of A in the final sulfurized CZTS thin films. By comparing the power conversion efficiency ( $\eta$ ) of these cells as shown in Fig. 11(a), it is found that the variations of efficiency in the cells with water vapor treatments are relatively smaller than that of the cells without treatment. The formation of cells with efficiency lower than 3% is also relatively fewer than that of the cells without water vapor treatment. The tendency of improvement is observed in all the samples A and B with treatments at  $250^\circ\text{C}$  and  $300^\circ\text{C}$  independent of their size, and especially the improvement is quite obvious in the cells B treated at  $300^\circ\text{C}$ . The efficiencies higher than 4% were achieved with good reproducibility in the cells B treated at  $300^\circ\text{C}$ . In contrast, the formation of dead cells is quite often in the samples without the treatment, especially in the larger cells. The formation of dead cells in the samples without treatments could be due to the existence of impurities or irregulars at the CZTS/CdS heterojunction, which may result in the formation of leak path. In comparing the open-circuit voltage ( $V_{oc}$ ) as shown in Fig. 11(b), the similar tendency of improvement is observed in the samples with treatments. The cells with  $V_{oc}$  larger than 600 mV are obtained in the samples treated at  $300^\circ\text{C}$  with good reproducibility independent of their size and composition. In the case of the samples with treatment at  $350^\circ\text{C}$ , the similar convergence of variation is observed, although an increase in the  $\eta$  and  $V_{oc}$  is not obtained. The improvement of  $\eta$  and  $V_{oc}$  with better reproducibility especially observed in the cells with treatments at  $250^\circ\text{C}$  and  $300^\circ\text{C}$  could be due to the effect of removing impurity

phases or passivation of the defects by the treatment. At such a higher treatment temperature as  $350^\circ\text{C}$ , the excess surface oxidation as observed by the XPS analysis discussed above could be the reason why the enhancement of the cell performance is hindered, while the reproducibility of the cell characteristic is improved. The effect of treatment on the short-circuit current density ( $J_{sc}$ ) is compared in Fig. 11(c). The convergence of variation is found in the treated samples as in the case of  $\eta$  and  $V_{oc}$ , especially at higher treatment temperatures. Although a small improvement of  $J_{sc}$  is observed in the cells B with treatments, there is an opposite tendency in that of the cells A. The difference in the changes due to the treatment in the cells A and cells B could be related to their difference in the chemical composition since the composition of Zn is higher in A than B. The decreasing of  $J_{sc}$  is more obvious in the cells A with larger area. The deterioration of  $J_{sc}$  in the cells A at higher treatment temperatures could be due to the formation of excess surface oxidation layer, which could form a barrier for minority carriers. At larger cells, this effect could be more significant due to the presence of higher sheet resistance at the top transparent conductive electrode in addition to the resistance of the excess oxide layer compared to the smaller cells. In analyzing the fill factor (FF) as shown in Fig. 11(d), a clear trend of converging as in the other parameters of the cells with treatments can also be seen. It is also found that the formation of cells with relatively lower FF is significantly avoided by the treatments. In Fig. 11(e), the comparison of the shunt resistance ( $R_{sh}$ ) is shown. Variation of  $R_{sh}$  is drastically suppressed in the treated samples. Especially, in the samples treated at higher temperatures, the formation of cells with relatively low  $R_{sh}$  is prevented significantly. This beneficial effect indicates that the origins of defects causing leak paths at the heterojunction interface are eliminated effectively by the treatment at high temperatures. For the series resistance ( $R_s$ ) of the cells, it is observed that the fluctuation is suppressed in the samples with treatments as shown in Fig. 11(f). It is also found that the  $R_s$  of the cells treated at  $300^\circ\text{C}$  exhibits the convergence at relatively lower values. In the case of samples treated at  $350^\circ\text{C}$ , a slight increase in  $R_s$  compared to that of the  $300^\circ\text{C}$  is observed. This result indicates that there could be an optimum treatment temperature around  $300^\circ\text{C}$ , in which the benefit due to the removal of defects by the treatment could be dominant over that of excess oxidation. From the results discussed above, it is clarified that the reproducibility of the characteristic of either the small or large active area cells with water vapor treatment is better than that of the samples with no treatment independent of their difference in the bulk compositions. The improvement in the reproducibility of photovoltaic characteristics in the samples with water vapor treatment could be due to the formation of homogeneous CZTS/CdS heterojunction. Since there are both  $\text{H}^+$  and  $\text{OH}^-$  ions in the ultrasonically generated water vapor, simultaneous reactions such as reduction and oxidation of the impurity phases could be expected. Due to the reduction reactions mainly by the  $\text{H}^+$  ions, the decomposition or passivation of impurities may be expected, while the oxidation reactions caused by the  $\text{OH}^-$  ions would result in the formation of oxides or hydroxides. Formation of an oxide layer with a suitable thickness near the surface of CZTS thin film (consequently at the CZTS/CdS heterojunction) could be effective in the passivation of leak paths but the existence of an excess oxide layer would be harmful and caused the degradation in the characteristic of the cells as in the case of treatment at  $350^\circ\text{C}$ . It is considered that the treatment up to  $300^\circ\text{C}$  could be beneficial due to possible passivation effects. Therefore, an optimal control of treatment temperature together with starting precursor composition would be necessary to realize a better photovoltaic performance.

To analyze the characteristic of each individual cell in detail, a comparison between the best cell for each condition is made as

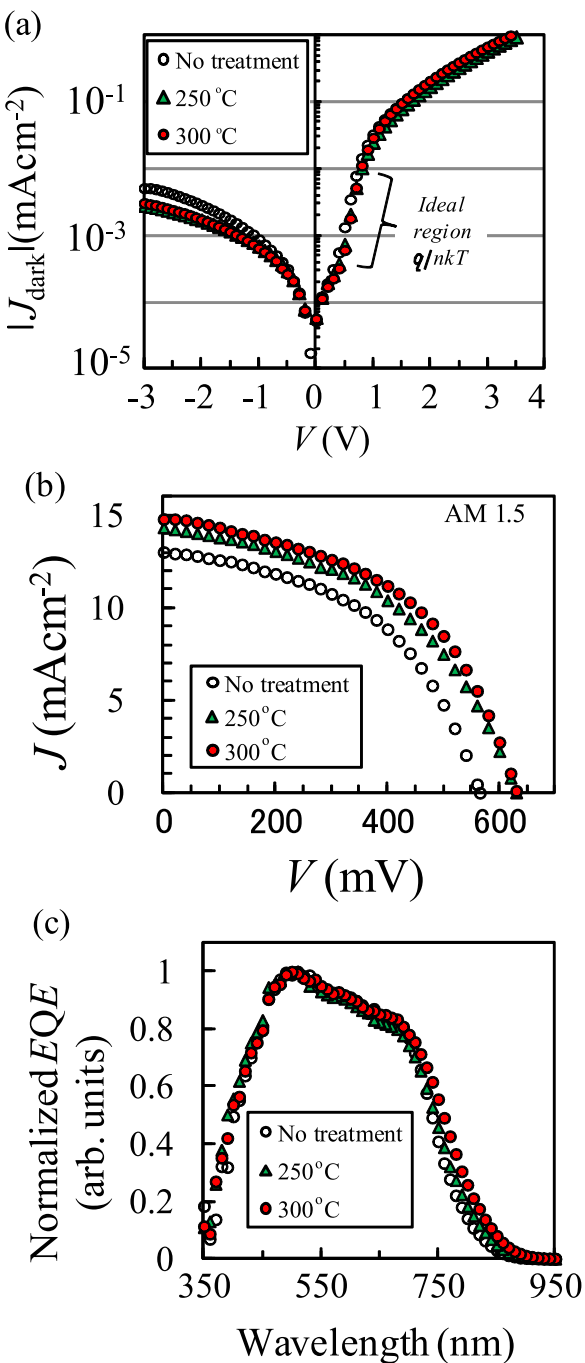


**Fig. 12.** The  $J$ - $V$  characteristics measured under (a) dark and (b) illumination of the sample without water vapor treatment (plotted in open-circle) comparing to those with the treatments at 250 °C (plotted in triangle) and 300 °C (plotted in red circle). All the dark-current densities,  $J_{\text{dark}}$ , at the reverse-bias voltage region are shown in absolute values for visual enhancement. The external quantum efficiencies,  $\text{EQE}$ , of the corresponding cells are shown in (c) with the same symbols. All the  $\text{EQE}$  spectra are normalized with respect to their corresponding maximum.

shown in Fig. 12 and Table 2. The current density ( $J$ ) versus voltage ( $V$ ) characteristics of the cells measured under the dark and AM 1.5 illumination are shown in Fig. 12(a) and (b) along with their corresponding external quantum efficiencies ( $\text{EQE}$ ) in Fig. 12(c), respectively. Based on the slope ( $q/nkT$ , where  $q$ ,  $k$ , and  $T$  refer to electronic charge, Boltzmann constant, and temperature, respectively) and the extrapolation of the ideal straight line region of the  $\ln(|J_{\text{dark}}|)$  vs.  $V$  plot of the cells measured under the dark as shown in Fig. 12(a), it is found that the ideal diode factor ( $n$ ) and reverse-

**Table 2**

The characteristics of the best cell without treatment compared to that of the best cells treated at 250 °C and 300 °C.

Parameters of the cells	Treatment conditions		
	No treatment	250 °C	300 °C
$n$	5.2	5.1	4.7
$J_0$ (mA/cm <sup>2</sup> )	$2.6 \times 10^{-3}$	$8.0 \times 10^{-4}$	$7.7 \times 10^{-4}$
$\eta$ (%)	3.6	4.2	4.5
$V_{\text{oc}}$ (mV)	565	630	632
$J_{\text{sc}}$ (mA/cm <sup>2</sup> )	13.0	14.4	14.6
$F.F$ (%)	48.3	46.3	48.7
$R_{\text{sh}}$ ( $\Omega$ cm <sup>2</sup> )	$1.9 \times 10^2$	$1.9 \times 10^2$	$2.0 \times 10^2$
$R_s$ ( $\Omega$ cm <sup>2</sup> )	11.0	11.0	10.7

saturation current density ( $J_0$ ) of the samples with the treatments are smaller than that of the sample without treatment. The decreasing of  $J_0$  refers to the reducing of leakage in the cell. This result indicates that the quality of heterojunction of the samples with treatment is improved, although they are still far from the characteristic of an ideal diode. In comparing the  $J$ - $V$  curves under illumination as shown in Fig. 12(b), it is found that the  $\eta$  of the best cell with treatment at 300 °C is increased to 4.5%, which is about 25% higher than that of the best cell without treatment. Other parameters such as  $V_{\text{oc}}$  and  $J_{\text{sc}}$  are also observed to be enhanced by over 10%. However, the changes in the  $R_{\text{sh}}$  and  $R_s$  are relatively indistinguishable. The improvement of  $V_{\text{oc}}$  and  $J_{\text{sc}}$  could be related to the passivation of defects at the heterojunction by the treatment. In analyzing the normalized  $\text{EQE}$  as shown in Fig. 12(c), an improvement in the long wavelength region is observed in the cells with treatments. This could be the indicative of enhancement of the absorber quality in the cells by the treatment because the spectral response is increased in a long wavelength region. This could be due to the passivation of defects at the interfaces of grain boundaries inside the CZTS thin films by the  $\text{H}^+$  ions from the ultrasonically generated water vapor, which may result in the improvement of collection of the carriers excited by the photons penetrating deep inside the absorber layer.

#### 4. Conclusions

The effect of surface treatment of the  $\text{Cu}_2\text{ZnSnS}_4$  thin-film absorbers utilizing water vapor generated by ultrasonic spray technique was analyzed. The effects of water vapor treatment on the crystalline properties and the surface morphology of CZTS thin films were difficult to confirm by the XRD, Raman, and SEM observations. The electrical resistivity of the CZTS thin films was observed to be stable in the range of  $10^3 \Omega \text{ cm}$  independent of the water vapor treatment. By the combination of elemental mapping and surface compositional analyses, it is concluded that the water vapor treatment is efficient in suppressing the unintentional fluctuation of the chemical composition near the surface region of CZTS thin films so that homogeneous deposition of CdS buffer layer could be realized. In the energy band alignment measurement, the structure of CZTS/CdS heterojunction was observed to be of the staggered type, i.e., both of the VBM and CBM of CZTS are higher than that of the CdS. It is also found that the effect on the variation of the discontinuities of VBM and CBM at the CZTS/CdS heterojunction due to the oxidation by the water vapor near the surface of CZTS thin films was less than  $\pm 50$  meV. The reproducibility of the photovoltaic characteristics was improved by water vapor treatment at moderate temperatures below 350 °C utilizing ultrasonic spray technique. The efficiency of solar cells higher than

4% was achieved in good reproducibility at the treatment temperature of 300 °C.

## Acknowledgments

The authors would like to thank Mr. Isamu Minemura for his great help in setting up the experimental equipments.

## References

- [1] B.M. Kayes, H. Nie, R. Twist, S.G. Spruytte, F. Reinhardt, I.C. Kizilyalli, G.S. Higashi, 27.6% Conversion efficiency, a new record for single-junction solar cells under 1 sun illumination, in: Proceedings of the 37th IEEE Photovoltaics Specialist Conference, 2011, p. 4, <http://dx.doi.org/10.1109/PVSC.2011.6185831>.
- [2] P. Jackson, D. Hariskos, E. Lotter, S. Paetel, R. Wuerz, R. Menner, W. Wischmann, M. Powalla, New world record efficiency for Cu(In,Ga)Se<sub>2</sub> thin-film solar cells beyond 20%, *Prog. Photovolt.: Res. Appl.* 19 (2011) 894.
- [3] M.A. Green, K. Emery, Y. Hishikawa, W. Warta, E.D. Dunlop, Solar cell efficiency tables (version 45), *Prog. Photovolt.: Res. Appl.* 23 (2015) 1.
- [4] M.T. Htay, T. Mandokoro, H. Seki, T. Sakai, N. Momose, T. Taishi, Y. Hashimoto, K. Ito, Influence of Ge composition in the Cu<sub>2</sub>Sn<sub>1-x</sub>Ge<sub>x</sub>S<sub>3</sub> thin-film photovoltaic absorber prepared by sulfurization of laminated metallic precursor, *Sol. Energy Mater. Sol. Cells* 140 (2015) 312.
- [5] M. Umehara, Y. Takeda, K. Ohishi, Y. Aoki, T. Motohiro, T. Sakai, R. Maekawa, Energy level diagram around Ge-rich grain boundaries in Cu<sub>2</sub>Sn<sub>1-x</sub>Ge<sub>x</sub>S<sub>3</sub> (CTGS) thin-film solar cells, *Sol. Energy Mater. Sol. Cells* 134 (2015) 1.
- [6] M. Umehara, Y. Takeda, T. Motohiro, T. Sakai, H. Awano, R. Maekawa, Cu<sub>2</sub>Sn<sub>1-x</sub>Ge<sub>x</sub>S<sub>3</sub>(x = 0.17) thin-film solar cells with high conversion efficiency of 6.0%, *Appl. Phys. Express* 6 (2013) 045501.
- [7] T. Mandokoro, M.T. Htay, N. Momose, T. Taishi, Y. Hashimoto, K. Ito, Preparation of Cu<sub>2</sub>Sn<sub>1-x</sub>Ge<sub>x</sub>S<sub>3</sub> thin-film alloys by sulfurization and their photovoltaic properties, in: Proceedings of the 4th International Symposium on Organic and Inorganic Electronic Materials and Related Nanotechnologies, P3–57, 2013.
- [8] M. Buffière, G. Brammertz, M. Batuk, C. Verbist, D. Mangin, C. Köble, J. Hadermann, M. Meuris, J. Poortmans, Microstructural analysis of 9.7% efficient Cu<sub>2</sub>ZnSnSe<sub>4</sub> thin film solar cells, *Appl. Phys. Lett.* 105 (2014) 183903.
- [9] G. Brammertz, M. Buffière, S. Oueslati, H. ElAnzeery, K.B. Messaoud, S. Sahayaraj, C. Köble, M. Meuris, J. Poortmans, Characterization of defects in 9.7% efficient Cu<sub>2</sub>ZnSnSe<sub>4</sub>–CdS–ZnO solar cells, *Appl. Phys. Lett.* 103 (2013) 163904.
- [10] I. Repins, C. Beall, N. Vora, C. DeHart, D. Kuciauskas, P. Dippo, B. To, J. Mann, W. C. Hsu, A. Goodrich, R. Noufi, Co-evaporated Cu<sub>2</sub>ZnSnSe<sub>4</sub> films and devices, *Sol. Energy Mater. Sol. Cells* 101 (2012) 154.
- [11] C.K. Miskin, W.C. Yang, C.J. Hages, N.J. Carter, C.S. Joglekar, E.A. Stach, R. Agrawal, 9.0% efficient Cu<sub>2</sub>ZnSn(S,Se)<sub>4</sub> solar cells from selenized nanoparticle inks, *Prog. Photovolt.: Res. Appl.* 23 (2015) 654.
- [12] K. Ito, Copper Zinc Tin Sulfide-Based, first ed., John Wiley & Sons Ltd., Chichester, 2015.
- [13] S. Oueslati, G. Brammertz, M. Buffière, H. ElAnzeery, O. Touayar, C. Köble, J. Bekeraert, M. Meuris, J. Poortmans, Physical and electrical characterization of high-performance Cu<sub>2</sub>ZnSnSe<sub>4</sub> based thin film solar cells, *Thin Solid Films* 582 (2015) 224.
- [14] K. Furuta, N. Sakai, T. Kato, H. Sugimoto, Y. Kurokawa, A. Yamada, Improvement of Cu<sub>2</sub>ZnSn(S,Se)<sub>4</sub> solar cell efficiency by surface treatment, *Phys. Status Solidi (c)* 12 (2015) 704.
- [15] W. Wang, M.T. Winkler, O. Gunawan, T. Gokmen, T.K. Todorov, Y. Zhu, D. B. Mitzi, Device characteristics of CZTS thin-film solar cells with 12.6% efficiency, *Adv. Energy Mater.* 4 (2014) 1301465.
- [16] B. Shin, O. Gunawan, Y. Zhu, N.A. Bojarczuk, S.J. Chey, S. Guha, Thin film solar cell with 8.4% power conversion efficiency using an earth-abundant Cu<sub>2</sub>ZnSnS<sub>4</sub> absorber, *Prog. Photovolt.* 21 (2013) 72.
- [17] T. Eguchi, T. Maki, S. Tajima, T. Ito, T. Fukano, Cu<sub>2</sub>ZnSnS<sub>4</sub> solar cells with 7.6% efficiency, Technical Digest, in: Proceedings of the 21st International Photovoltaic Science and Engineering Conference, <sup>4</sup>D-3P-24, 2011.
- [18] N. Momose, M.T. Htay, T. Yudasaka, S. Igarashi, T. Seki, S. Iwano, Y. Hashimoto, K. Ito, Cu<sub>2</sub>ZnSnS<sub>4</sub> thin film solar cells utilizing sulfurization of metallic precursor prepared by simultaneous sputtering of metal targets, *Jpn. J. Appl. Phys.* 50 (2011) 01BG09.
- [19] A. Ennaoui, M. Lux-Steiner, A. Weber, D. Abou-Ras, I. Kötchau, H.-W. Shock, R. Schurr, A. Höling, S. Jost, T. Voß, J. Schulze, A. Kirbs, Cu<sub>2</sub>ZnSnS<sub>4</sub> thin film solar cells from electroplated precursors Novel low-cost perspective, *Thin Solid Films* 517 (2009) 2511.
- [20] M. Courel, J.A. Andrade-Arvizu, O. Vigil-Galán, Towards a CdS/Cu<sub>2</sub>ZnSnS<sub>4</sub> solar cell efficiency improvement: a theoretical approach, *Appl. Phys. Lett.* 105 (2015) 233501.
- [21] W. Shockley, H.J. Queisser, Detailed balance limit of efficiency of p-n junction solar cells, *J. Appl. Phys.* 32 (1961) 510.
- [22] Z.Y. Dong, Y.F. Li, B. Yao, Z.H. Ding, G. Yang, R. Deng, X. Fang, Z.P. Wei, L. Liu, An experimental and first-principles study on band alignments at interfaces of Cu<sub>2</sub>ZnSnS<sub>4</sub>/CdS/ZnO heterojunctions, *J. Phys. D: Appl. Phys.* 47 (2014) 075304.
- [23] A. Santoni, F. Biccari, C. Malerba, M. Valentini, R. Chierchia, A. Mittiga, Valence band offset at the CdS/Cu<sub>2</sub>ZnSnS<sub>4</sub> interface probed by x-ray photoelectron spectroscopy, *J. Phys. D: Appl. Phys.* 46 (2013) 175101.
- [24] J. Li, Q. Du, W. Lui, G. Jiang, X. Feng, W. Zhang, J. Zhu, C. Zhu, The band offset at CdS/Cu<sub>2</sub>ZnSnS<sub>4</sub> heterojunction interface, *Electron. Mater. Lett.* 8 (2012) 365.
- [25] W. Bao, M. Ichimura, First-principles study on influences of crystal structure and orientation on band offsets at the CdS/Cu<sub>2</sub>ZnSnS<sub>4</sub> interface, *Int. J. Photoenergy* 2012 (2012) 619812.
- [26] S. Tajima, K. Kataoka, N. Takahashi, Y. Kimoto, T. Fukano, M. Hasegawa, H. Hazama, Direct measurement of band offset at the interface between CdS and Cu<sub>2</sub>ZnSnS<sub>4</sub> using hard X-ray photoelectron spectroscopy, *Appl. Phys. Lett.* 103 (2013) 243906.
- [27] M. Bär, B.-A. Schubert, B. Marsen, R.G. Wilks, S. Pookpanratana, M. Blum, S. Krause, T. Unold, W. Yang, L. Weinhardt, C. Heske, H.-W. Shock, Cliff-like conduction band offset and KCN-induced recombination barrier enhancement at the CdS/Cu<sub>2</sub>ZnSnS<sub>4</sub> thin-film solar cell heterojunction, *Appl. Phys. Lett.* 99 (2011) 222105.
- [28] C. Yan, F. Liu, N. Song, B.K. Ng, J.A. Stride, A. Tadich, X. Hao, Band alignments of different buffer layers (CdS, Zn(O,S), and In<sub>2</sub>S<sub>3</sub>) on Cu<sub>2</sub>ZnSnS<sub>4</sub>, *Appl. Phys. Lett.* 104 (2014) 173901.
- [29] R. Haight, A. Barkhouse, O. Gunawan, B. Shin, M. Copel, M. Hopstaken, D. B. Mitzi, Band alignment at the Cu<sub>2</sub>ZnSn(S<sub>x</sub>Se<sub>1-x</sub>)<sub>4</sub>/CdS interface, *Appl. Phys. Lett.* 98 (2011) 253502.
- [30] N. Momose, M.T. Htay, K. Sakurai, S. Iwano, Y. Hashimoto, K. Ito, Cu<sub>2</sub>ZnSn(S<sub>x</sub>Se<sub>1-x</sub>)<sub>4</sub> thin-film solar cells utilizing simultaneous reaction of a metallic precursor with elemental sulfur and selenium vapor sources, *Appl. Phys. Express* 5 (2012) 081201.
- [31] D. Aaron, R. Barkhouse, R. Haight, N. Sakai, H. Hiroi, H. Sugimoto, D.B. Mitzi, Cd-free buffer layer materials on Cu<sub>2</sub>ZnSn(S<sub>x</sub>Se<sub>1-x</sub>)<sub>4</sub>: band alignments with ZnO, ZnS and In<sub>2</sub>S<sub>3</sub>, *Appl. Phys. Lett.* 100 (2012) 193904.
- [32] H. Katagiri, K. Jimbo, S. Yamada, T. Kamimura, W.S. Maw, T. Fukano, T. Ito, T. Motohiro, Enhanced conversion efficiencies of Cu<sub>2</sub>ZnSnS<sub>4</sub>-based thin film solar cells by using preferential etching technique, *Appl. Phys. Express* 1 (2008) 041201.
- [33] H. Miyazaki, M. Aono, H. Kishimura, H. Katagiri, Effect of surface treatment of CZTS absorber layer by ammonia solution, *Phys. Status Solidi (c)* 12 (2015) 745.
- [34] H. Miyazaki, M. Aono, H. Kishimura, H. Katagiri, Effects of preferential etching treatment of CZTS absorber layer by deionized water, *Phys. Status Solidi (c)* 12 (2015) 749.
- [35] H. Miyazaki, M. Aono, H. Kishimura, H. Katagiri, Surface etching of CZTS absorber layer by Br-related solution, *Phys. Status Solidi (c)* 12 (2015) 741.
- [36] A. Fairbrother, E. Graecia-Hemme, V. Izquierdo-Roza, Z. Frontané, F. A. Pulgarín-Agüedó, O. Vigil-Galán, A. Pérez-Rodríguez, E. Saucedo, Development of a selective chemical etch to improve the conversion efficiency of Zn-rich Cu<sub>2</sub>ZnSnS<sub>4</sub> solar cells, *J. Am. Chem. Soc.* 134 (2012) 8018.
- [37] M.T. Htay, Y. Hashimoto, N. Momose, K. Sasaki, H. Ishiguchi, S. Igarashi, K. Sakurai, K. Ito, A cadmium-free Cu<sub>2</sub>ZnSnS<sub>4</sub>/ZnO heterojunction solar cell prepared by practicable processes, *Jpn. J. Appl. Phys.* 50 (2011) 032301.
- [38] M.T. Htay, M. Okamura, R. Yoshizawa, Y. Hashimoto, K. Ito, Synthesis of a cuprite thin film by oxidation of a Cu metal precursor utilizing ultrasonically generated water vapor, *Thin Solid Films* 556 (2014) 211.
- [39] M.T. Htay, Y. Hashimoto, Field emission property of ZnO nanowires prepared by ultrasonic spray pyrolysis, *Superlatt. Microstruct.* 84 (2015) 144.
- [40] M.T. Htay, Y. Hashimoto, K. Ito, Growth of ZnO submicron single-crystalline platelets, wires, and rods by ultrasonic spray pyrolysis, *Jpn. J. Appl. Phys.* 46 (2007) 440.
- [41] Y. Hashimoto, K. Takeuchi, K. Ito, Band alignment at CdS/CuInS<sub>2</sub> heterojunction, *Appl. Phys. Lett.* 67 (1995) 980.
- [42] D.M. Berg, M. Arasimowicz, R. Djemour, L. Gülay, S. Siebentritt, S. Schorr, X. Fontané, V. Izquierdo-Roca, A. Pérez-Rodríguez, P.J. Dale, Discrimination and detection limits of secondary phases in Cu<sub>2</sub>ZnSnS<sub>4</sub> using X-ray diffraction and Raman spectroscopy, *Thin Solid Films* 569 (2014) 113.